Journal of Anatomy

J. Anat. (2009) **214**, pp153–162 doi: 10.1111/j.1469-7580.2008.01003.x

Morphological and biochemical analyses of otoliths of the ice-fish *Chionodraco hamatus* confirm a common origin with red-blooded species

Chiara Maria Motta,[1] Bice Avallone,[1] Giuseppina Balassone,[2] Giuseppe Balsamo,[1] Umberto Fascio,[3] Palma Simoniello,[1] Stefania Tammaro[1] and Francesco Marmo[1]

[1]*Department of Biological Sciences and*
[2]*Department of Earth Science, University of Naples Federico II, Naples, Italy*
[3]*C.I.M.A. University of Milan, Italy*

Abstract

The morphology and composition of the three otoliths of the Antarctic ice-fish *Chionodraco hamatus* were studied by scanning electron microscopy and X-ray diffraction. The composition of the sagitta, lapillus and asteriscus protein matrices was also analysed by sodium dodecyl sulphate-polyacrylamide gel electrophoresis, western blots and confocal laser scanning microscopy to reveal the presence of and to localize the calcium-binding proteins calmodulin, calbindin and S-100. Morphological results indicated that the otoliths in this ice-fish were similar to those of *Trematomus bernacchii*, a red-blooded Antarctic species [B. Avallone et al. (2003) *J. Submicrosc. Cytol. Pathol.* **35**, 69–76], but rather different from those of other teleosts. These two Antarctic species possessed a completely vateritic asteriscus, whereas their sagitta and lapillus were made mostly of aragonite. Parallel analysis of protein patterns in *C. hamatus* and *T. bernacchii* revealed that the sagitta significantly differed from the lapillus and asteriscus in both species. The sagitta did not contain the S-100 protein and showed calmodulin and calbindin located in discontinuous or incremental zones, respectively. These results demonstrate that the otoliths of *C. hamatus* and *T. bernacchii* share more resemblances than differences and support the idea of a common origin of these species.
Key words calcium-binding proteins; confocal laser scanning microscopy; crystalline morph; matrix protein composition; *Trematomus bernacchii*.

Introduction

Otoconia are crystalline structures localized in the vestibular macular organs. In bony fishes, they are the mechanical components of the sound transduction system, responsible for hearing (Parker, 1908; Schuijf, 1981; Fay, 1984) and vestibular function. In these vertebrates they have a complex organization consisting of an organic matrix on which inorganic calcium carbonate is deposited (Henle, 1873), with the consequent formation of complex architectures that are used for systematic purposes. With regard to this, the gross and fine morphology of otoliths has been described in many species (Lewis & Nemanic, 1972; Morales-Nin, 1985; Lombarte et al. 1991; Gauldie, 1993) including the red-blooded Antarctic species *Trematomus bernacchii* (Avallone et al. 2003).

In this species the fine morphology and crystalline morph of the saccular (sagitta), utricular (lapillus) and lagena (asteriscus) otoliths have been described, revealing that the sensory faces are finely decorated and show different sculpturing. The same study demonstrated that the sagitta and lapillus are aragonitic, whereas the asteriscus is vateritic (Avallone et al. 2003).

In the present work we describe the morphology and composition of the three otoliths of *Chionodraco hamatus*, a haemoglobin-free Channichthyid. The morphological analysis was carried out by scanning electron microscopy, whereas the crystalline morph was determined by X-ray diffraction. Our observations were compared with those previously described for the sagitta, lapillus and asteriscus of *T. bernacchii* (Avallone et al. 2003).

Comparison between the two species was also extended to the biochemical level by analysis of the protein pattern of the water-soluble matrix present in the otoliths by gel electrophoresis. Although the precise composition of the organic phase of otoconia is unknown, it clearly consists of proteins and carbohydrates (Wislocki & Ladman, 1955; Bèlanger, 1960; Marmo et al. 1964; Ross et al. 1985; Gil-Loyzaga et al. 1985). The organic matrix is probably involved in regulating crystal seeding and growth by initiating and/or controlling the subsequent rates of carbonate

Correspondence
Chiara M. Motta, Dipartimento delle Scienze Biologiche, Sezione di Biologia Evolutiva e Comparata, Via Mezzocannone 8, 80134 Napoli, Italy. E: mottacm@unina.it

Accepted for publication *19 September 2008*

deposition (Piscopo et al. 2003). Effectively, the protein type would determine the type of crystal polymorph formed (Lowenstam & Weiner, 1989). This hypothesis was confirmed by Pote and Ross (1986, 1991), who have shown that each mineral polymorph of otoconia contains proteins unique to that polymorph.

It has been suggested that calcium-binding proteins may modulate calcium-associated events by regulating intracellular levels of calcium (Yamashita et al. 1995). It is not surprising therefore that calmodulin (CaM) has been identified in the cochlea of gerbil (Nakazawa, 2001) and guinea pig (Furness et al. 2002), and that calbindin-D28-K (CaB) has been found in the primate (Usami et al. 1995) and chick (Hiel et al. 2002) inner ear, in the dog cochlea (Coppens et al. 2000) and in the otoconia of the musk shrew (Karita et al. 1999). In the lizard *Podarcis sicula*, CaB is present on the outer surface, in the central core (Balsamo et al. 2000) and in the organic matrix of otoconia (Piscopo et al. 2003, 2004). CaM, CaB, S-100 and parvalbumin are all parts of the uncalcified organic mass that holds otoconia together in the brook lamprey *Lampetra planeri* (Avallone et al. 2005). In this study we investigated the presence of CaB, CaM and S-100 in the otolith extracts obtained from *C. hamatus* by immunoblotting and also, for comparison, from *T. bernacchii*. The localization of CaB and CaM in the three different otoconia was determined in both species by confocal laser scanning microscopy.

Materials and methods

Animals

Five adult female *C. hamatus* specimens (ranging between 40 and 44 cm) and six adult female *T. bernacchii* specimens (between 18 and 31 cm) were caught in Terra Nova Bay close to the Italian Station in Antarctica (74°41′ 42″ S, 164°07′ 23″ E). Otoliths were removed from animals anaesthetized with tricaine methanesulfonate (MS-222, 200 μM) and the gelatinous layer of the otolithic membrane was carefully peeled from the sensory epithelium. They were quick frozen and stored dry at –80 °C until arrival at the laboratories in Italy. Otoliths removed from different fish were randomly allotted for scanning electron microscopy (three samples from *C. hamatus*), confocal laser scanning microscopy (three samples from *C. hamatus*; three samples from *T. bernacchii*), X-ray diffraction (two samples from *C. hamatus*) or biochemical analyses (two samples from *C. hamatus*; three samples from *T. bernacchii*).

Scanning electron microscopy

Otoliths were rinsed for 24 h in 1% sodium dodecyl sulphate to remove contaminants from the sensory epithelium. A group of specimens was mildly etched in 0.1 M EDTA for 20 h to expose the crystal surface (Avallone et al. 2003). All specimens were then dehydrated in a graded sequence of ethanol and ethanol/Freon mixture to 100% Freon and critical-point dried. Samples were then attached to their stubs and coated with carbon and gold for 30 s at a distance of 15 cm from the source at 40 kV and 2–3 mA. Observations were carried out with a Cambridge Stereoscan 250 MK II microscope.

X-ray diffraction

The mineralogical composition of unfixed otoliths was determined by means of X-ray powder diffraction patterns using an automated diffractometer (MZVI, Seifert) (CuKα radiation 1.5418 Å, 40 kV and 30 mA; 2θ range 22 and 52°; 0.5° 2θ min^{-1} speed). The program (Rayflex, GE Inspection Technologies) was used to evaluate the profiles and the results were compared with International Centre for Diffraction Data (ICDD) database.

Protein extraction and analysis

Single otoliths were crushed with a pestle in 0.9% NaCl and then centrifuged for 5 min at 11,200 g in a centrifuge (model 5415D, Eppendorf) at 4 °C. Otoconia were resuspended in 500 μL of 2% sodium dodecyl sulphate, 0.1 M sodium acetate, pH 7.4, 1.5 μg mL^{-1} leupeptin, 1 μg mL^{-1} pepstatin, 1 mM EDTA and 1 mM phenylmethylsulphonyl fluoride, sonicated for 2 min at 180 W and centrifuged for 5 min at 11,200 g at 4 °C. This extraction step was repeated three times and the three resulting supernatants were pooled. Both the supernatants and final pellets were incubated for 2 h at 4 °C in 5% EDTA, dialysed against 10 mM $MgCl_2$ in the presence of protease inhibitors (see above) and thoroughly rinsed in double-distilled water. The dialysate obtained was lyophilized.

Samples were analysed by sodium dodecyl sulphate–polyacrylamide gel electrophoresis to determine their protein content. Polyacrylamide gels (12.5%) were run in Tris-glycine buffer (Laemmli, 1970) and stained with silver nitrate (Merril et al. 1984).

Immunoblotting

Immediately after electrophoresis, gels were blotted onto nitrocellulose paper (0.45 μm pore; Amersham, Milan, Italy) for 2 h at 100 V at 4 °C in a blotting chamber filled with transfer buffer (20% methanol, 0.025 mM Tris-base, 0.129 M glycine, pH 8.5). Blotted membranes were washed in 3% low-fat powdered milk in 0.1 M phosphate-buffered saline (PBS), pH 7.2, for 60 min at 37 °C to reduce non-specific binding. They were then incubated with monoclonal anti-CaB (clone CB-955, 1:2500, Sigma, St Louis, MO, USA), monoclonal anti-CaM (clone 6D4, 1:1000, Sigma) or monoclonal anti-S-100 (clone SH-B1, 1:1000, Sigma) in PBS for 2 h at 37 °C. After three washes with PBS, blots were incubated with the secondary antibody, a horseradish peroxidase-conjugated rabbit anti-mouse IgG (1:1000, Sigma), for 1 h at 37 °C. After repeated washes with PBS, blots were placed in 10 mL of methanol containing 3 mg mL^{-1} 4-chloro-1-naphthol and 10 μL of 30% (v/v) H_2O_2. Membranes were kept under constant motion until bands appeared and were then washed with double-distilled water. Samples treated with pre-immune sera, used as negative controls, were always completely unstained (data not shown).

Confocal laser scanning microscopy

Otoliths fixed in absolute methanol at 4 °C for 2 h were treated with 0.25% Triton-X100 and 0.1% Tween20 in 0.1 M PBS (pH 7.4) for 1 h. After several rinses in PBS, they were incubated overnight at 4 °C with rabbit anti-CaB (KD-15, 1:500, Sigma) and mouse monoclonal anti-CaM (clone 6D4, 1:1000, Sigma). After rinsing in PBS (6 × 10 min), the otoliths were incubated with 0.1 M PBS (pH 7.4) containing sheep anti-rabbit IgG conjugated with fluorescein isothiocyanate (FITC) (1:10) and sheep anti-mouse IgG conjugated with rhodamine (1:10) in a moist dark chamber for 2 h at room temperature (20 °C). After several rinses in PBS, the otoliths were mounted on

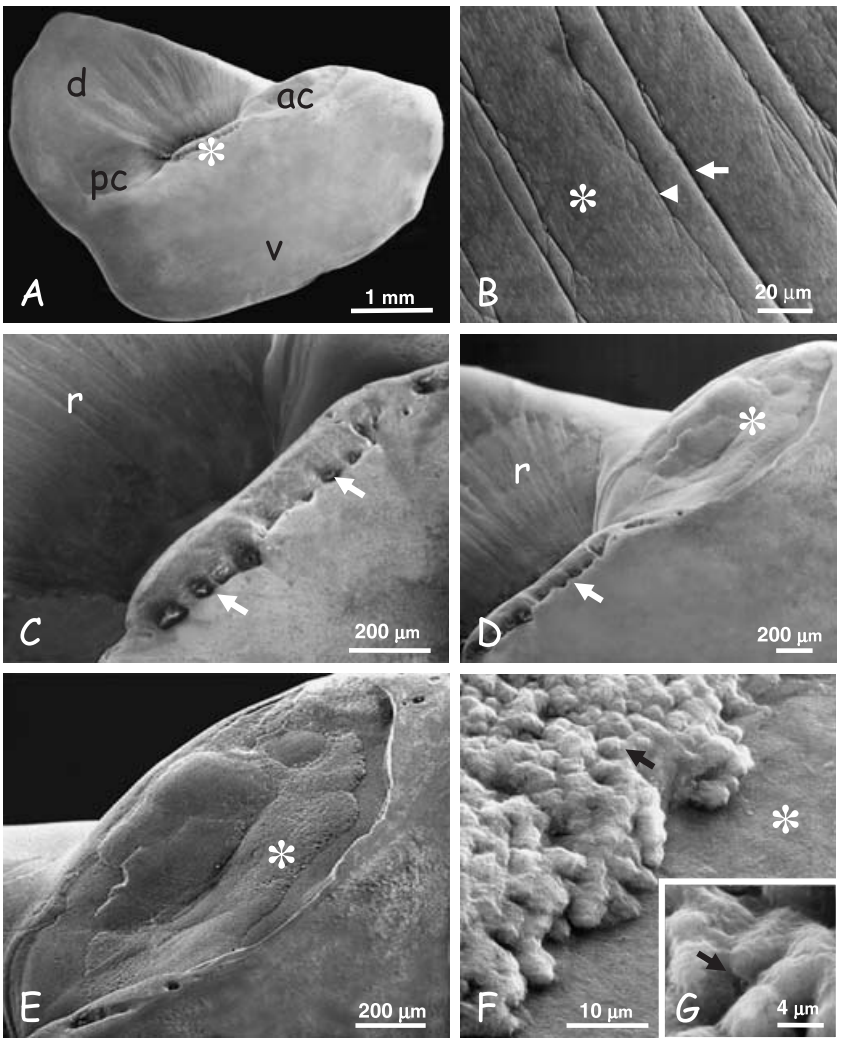

Fig. 1 Scanning electron micrographs of the sagitta in *C. hamatus*. (A) Whole otolith seen from the sensorial face. The anterior and posterior collicula (ac and pc) are visible together with the decorated collum (*). The dorsal (d) region shows radial ridges and the region ventral (v) to the sulcus acusticus is smooth and not decorated. (B) Detail of the dorsal region showing primary (arrow) and smaller secondary (arrowhead) depressions. Notice also the flat aspect of the ridge (*). (C) Collum decorated by a series of round depressions of various sizes and depths (arrows). r, radial ridges. (D) Collum (arrow) and anterior colliculum (*). Notice the elliptical shape, shallow depth and presence of an irregular, decorated bottom. R, ridges. (E) Detail of the anterior colliculum. The decorated bottom (*) is clearly evident. (F) Detail of the decoration. Notice that it is composed of a layer of grossly granular units (arrow) emerging from a smooth floor (*). (G) Detail of the granular units. They clearly differ in size, are separated by deep depressions (arrow) and often merge to form larger structures.

slides with diazabicyclo-octane (Sigma). Samples treated only with pre-immune sera were used as negative controls.

Observations were carried out under a confocal microscope (TCSNT, Leica) with laser argon/krypton 7.5 mW multilines. Focal series of horizontal planes of sections were simultaneously monitored for FITC using the 488- and 568-nm laser line, an FITC band-pass 530/30, and a long-pass filter 590 for tetramethyl rhodamine isothiocyanate (TRITC). The microscope was equipped with an acousto-optical tunable filter (AOTF) to minimize cross-talk during simultaneous detection of FITC/TRITC labels.

Results

Scanning electron microscopy of the sagitta in *C. hamatus*

At low magnification the saccular otolith, the sagitta, was seen as a large structure (4.2 × 3.8 mm) that was laterally compressed and elongated in the anterior/posterior axis. Seen from the side, it showed a grossly triangular profile with the anterior region appearing more developed and forming a rostrum. The contour lacked spines or evident protrusions (Fig. 1A).

The non-sensorial face was smooth and not decorated (images not shown), whereas the sensorial face was characterized by the presence of a sulcus acusticus clearly dividing the dorsal and ventral regions. The sulcus presented two large and elongated collicula separated by an obvious collum. The dorsal portion of the otolith showed ridges radiating from the collum and the ventral region was flat and homogeneous (Fig. 1A).

At higher magnification the dorsal region appeared smooth and was decorated by superficial depressions with no apparent correlation with the inner growth marks. Depressions were about 50 μm apart and delimited by flat ridges (Fig. 1B). Primary and secondary depressions could be recognized, the former uniquely departing from the collum and reaching the dorsal margin of the otolith. The secondary depressions, by contrast, were shorter, more irregular and superficial.

The collum was prominent and decorated by eight to 10 round depressions situated close to the edge (Fig. 1C). These depressions differed in size and depth but were equidistant to the rim and close to the deep depression limiting the collum from the radial area.

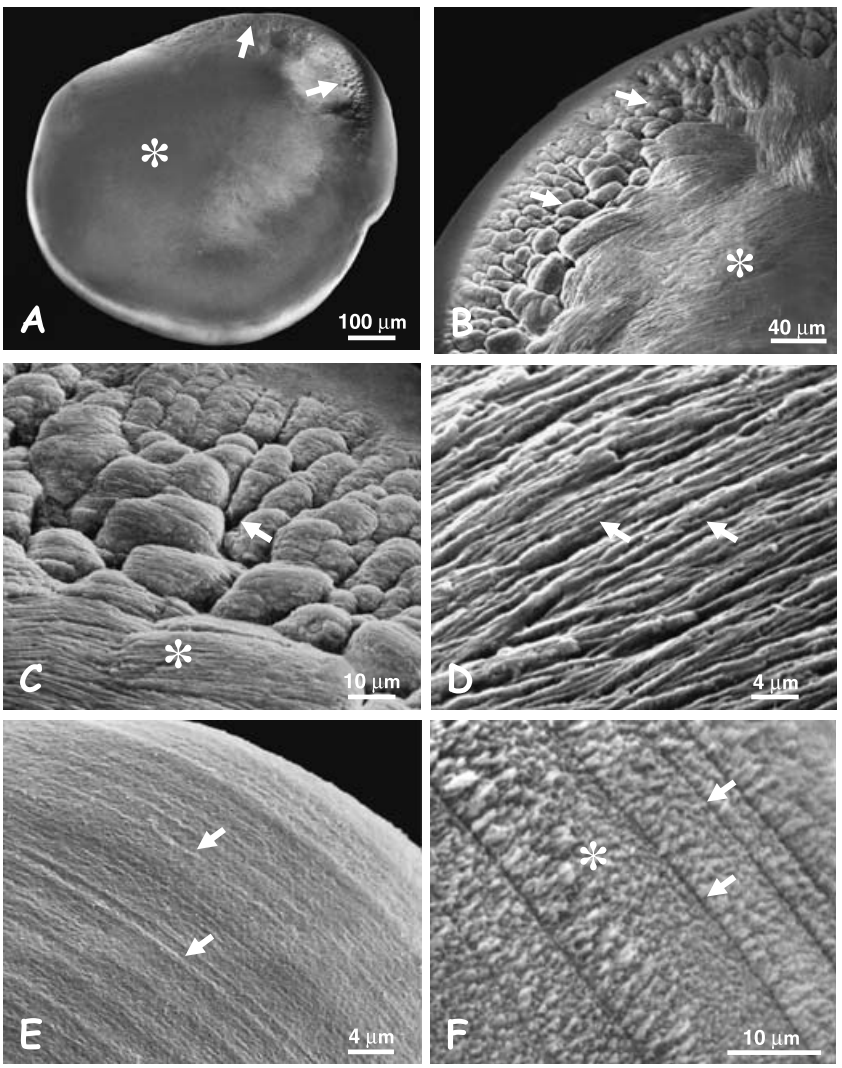

Fig. 2 Scanning electron micrographs of the lapillus in *C. hamatus*. (A) Sensory face characterized by the presence of a central depression (*) and a horseshoe band decorating the margin (arrows). Notice the rounded contours. (B) Detail of the band. The units show different sizes (arrows) and are separated by sharp discontinuities. The units and the region close to the band (*) appear filamentous. (C) Higher magnification of B. All units show a smooth contour; those located closer to the margin appear smaller and more regularly orientated. Discontinuities (arrow) are evident as well as the filamentous organization (*) of the whole structure. (D) Detail of the filaments (arrows) showing their regular distribution in bundles. (E) Margin of the otolith opposite to the decorated band. The growth increments (arrows) are visible. (F) Detail of E showing the incremental zones (*) characterized by spiny habit and discontinuous zones (arrows).

The two collicula were mild depressions that were elliptical in shape and located immediately beside the collum (Fig. 1D). Both were regularly outlined and contained a decorated and irregular bottom (Fig. 1E). Higher magnification revealed a 10 μm thick layer of 3–5 μm units, separated by depressions (Fig. 1F and G). This layer did not reach the edges of the collicula, where a finely homogeneous, non-decorated floor was evident (Fig. 1F).

Scanning electron microscopy of the lapillus in *C. hamatus*

In this species, the utricular otolith, the lapillus, had a conical shape with a diameter at the base of about 1.3 mm (Fig. 2A). The conical, non-sensorial face was decorated by the presence of small (< 1 μm) and homogeneous granular units (data not shown). The sensorial face was flat, characterized by the presence of a shallow central depression and decorated, close to the edge, by a horseshoe-shaped band (Fig. 2A and B) composed of large units (Fig. 2C). These were regularly placed but variable in shape and size, showing a smooth profile and separated by sharp discontinuities (Fig. 2B and C).

These units and the area close to the band showed a surface characterized by the presence of bundles of tiny filamentous structures approximately 1.5 μm thick and 15 μm long. They were orientated in parallel and were formed by small, regularly arranged granular crystals (Fig. 2D). In the remaining portion of the lapillus the growth increments, consisting of incremental and discontinuous zones, were clearly recognisable (Fig. 2E and F). At higher magnification, the incremental zones showed a spiny appearance (Fig. 2F).

Scanning electron microscopy of the asteriscus in *C. hamatus*

The asteriscus, present in the lagena, was a small and flat otolith (average 1.3×0.9 mm). Seen from the sensorial face it was kidney shaped with an emerging crescent that grossly divided the structure into three parts (Fig. 3A).

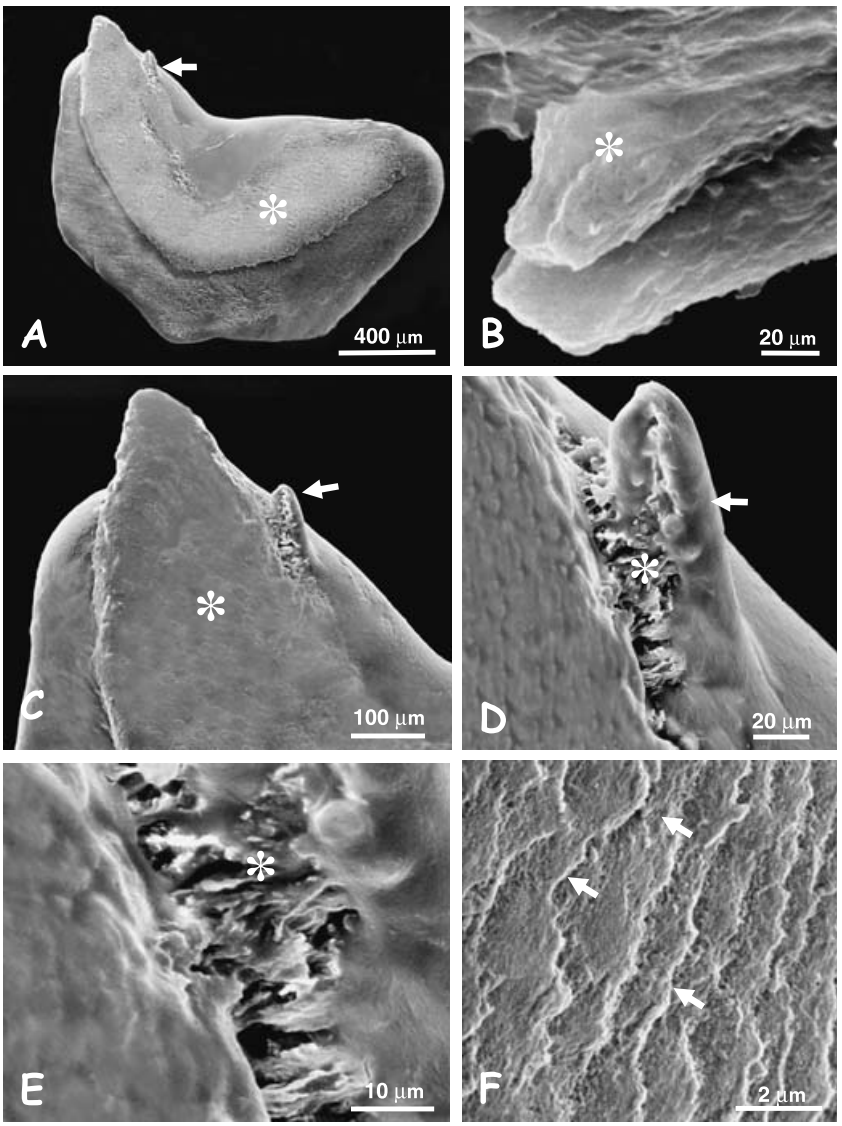

Fig. 3 Scanning electron micrographs of the asteriscus in *C. hamatus*. (A) Otolith showing the kidney shape, protruding crescent band (*) and long spine (arrow). (B) High magnification of the small spines (*) decorating the edge of the crescent area. (C) Detail of A. Notice the long spine (arrow) and the protruding crescent area (*). (D) Detail of the spine revealing the smooth superior surface (arrow) and presence, in the lower part, of a series of filamentous structures (*). (E) Detail of the filamentous structures (*). (F) Ring marks (arrows) appearing close to the otolith contours following mild EDTA etching.

This emergence was delimited by particularly steep edges decorated by 10–15 μm long spines that protruded from the contour (Fig. 3B). A longer and thicker spine was also present along the inner contour of the crescent area (Fig. 3C and D). Superiorly, this spine showed a smooth surface, whereas the lower part was connected to the crescent area by processes that gave it a filamentous appearance (Fig. 3D and E). The surface of the whole crescent area was decorated by large round smooth-surfaced units (Fig. 3D and E). Other portions of the otolith appeared smooth and scarcely decorated. At higher magnification, and following a mild EDTA etching, the growth marks appeared (Fig. 3F).

X-ray diffraction of the three otoliths of *C. hamatus*

All of the otoliths examined were composed of calcium carbonate, represented by the three polymorphs, aragonite, vaterite and calcite. The composition of the asteriscus was entirely of vaterite, whereas the lapillus and sagitta were heterogeneous. The former was mostly composed of aragonite with traces of calcite, as demonstrated by the small but sharp peak corresponding to 3.03 Å in the X-ray spectra (29.45° 2θ), and the latter was composed of a mixture of aragonite and vaterite (Fig. 4).

Protein patterns of the otolith matrix in *C. hamatus* and *T. bernacchii*

Matrices of the three otoliths were examined in *C. hamatus* and, for comparison, in *T. bernacchii*. The results showed that, in the two species, the asteriscus and lapillus had highly comparable protein patterns that were completely different from that observed in the sagitta. In particular, the asteriscus and lapillus contained four main proteins at 100, 40, 28 and 14 kDa and additional, less evident, bands

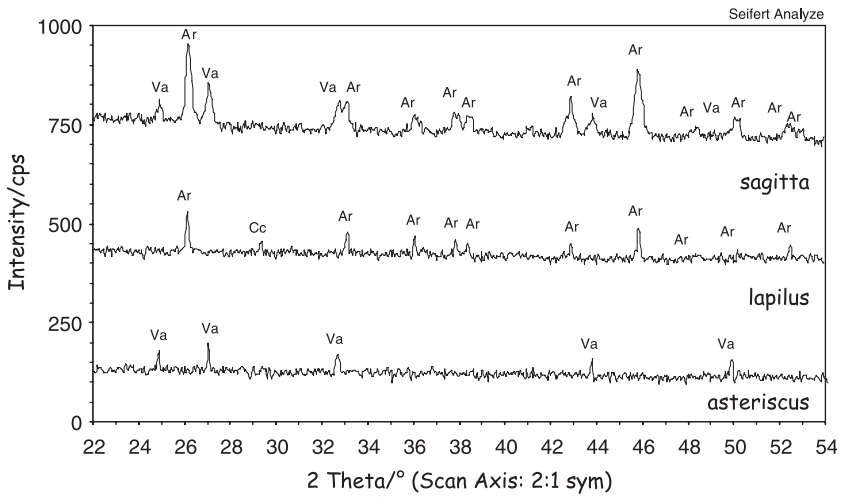

Fig. 4 Otolith composition in *C. hamatus* as determined by X-ray diffraction. Spectra demonstrate that the asteriscus is composed exclusively of vaterite (Va), the lapillus mostly of aragonite (Ar) with traces of calcite (Cc) and the sagitta of a mixture of aragonite and vaterite.

at about 58, 54, 49, 47, 43 and 37 kDa (Fig. 5A). The sagitta, in both *C. hamatus* and *T. bernacchii*, contained three main bands of approximately 50, 28 and 14 kDa and less evident bands at about 65, 62, 58, 45 and 38 kDa (Fig. 5A).

Immunoblotting

Immunoreactivity to CaB and CaM was present in *C. hamatus* and *T. bernacchii* in the sagitta, lapillus and asteriscus (Fig. 5B). In contrast, S-100 immunoreactivity was present only in samples obtained from the asteriscus and lapillus (Fig. 5C).

Confocal laser scanning microscopy

The CaM and CaB immunoreactivity was also present in the sagitta, lapillus and asteriscus of both species examined (Fig. 6). In the sagitta it was evident as an alternating green/red staining. The incremental zones were stained green by the anti-CaB antibody (Fig. 6A1, A3, B1 and B3), whereas the discontinuous zones were stained red by the anti-CaM antibody (Fig. 6A2, A3, B2 and B3). However, in the lapillus (Fig. 6C1–C3 and D1–D3) and asteriscus (Fig. 6E1–E3 and F1–F3) both CaM and CaB were present in the incremental zone, whereas the discontinuous zones lacked any immunoreactivity. The correspondence of the incremental and discontinuous zones with labelling in the sagitta and asteriscus is shown in Fig. 7A and B and C and D, respectively.

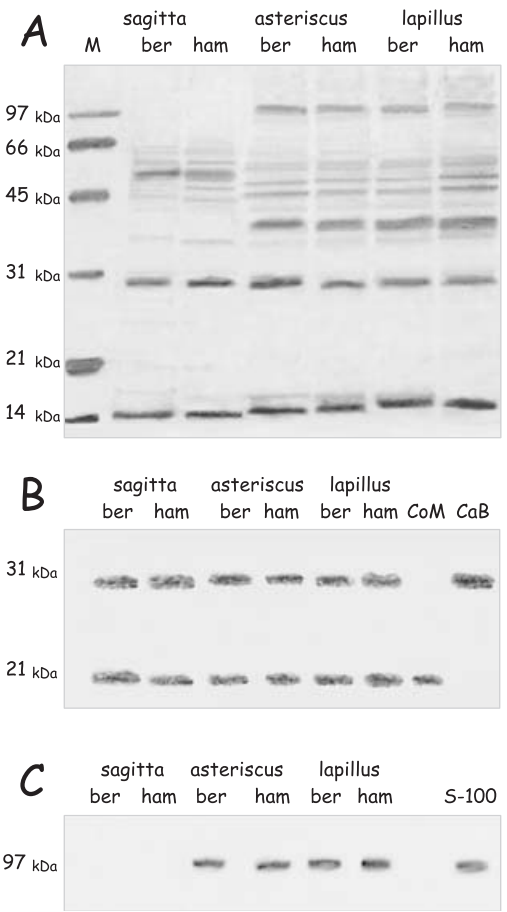

Fig. 5 Analysis of proteins present in otolith matrices. (A) Sodium dodecyl sulphate–polyacrylamide gel electrophoresis. Molecular weight standards (M) and proteins extracted from the sagitta, asteriscus and lapillus of *T. bernacchii* (ber) and *C. hamatus* (ham), respectively. (B) Immunoblot assay for CaB and CaM on the same samples as shown in A plus CaM and CaB as positive controls. All samples contain both proteins. (C) Immunoblot assay for S-100 on the same samples as shown in A plus S-100 as positive control. The protein is present only in the asteriscus and lapillus.

Discussion

Morphological observations indicate that, although the otoliths of *C. hamatus* closely resemble those of *T. bernacchii* (Avallone et al. 2003), minor differences also exist. In both species, the saccular otoliths, the sagittae, are compact with regular contours but appear different from those described in most other teleosts in which spines and/or marked

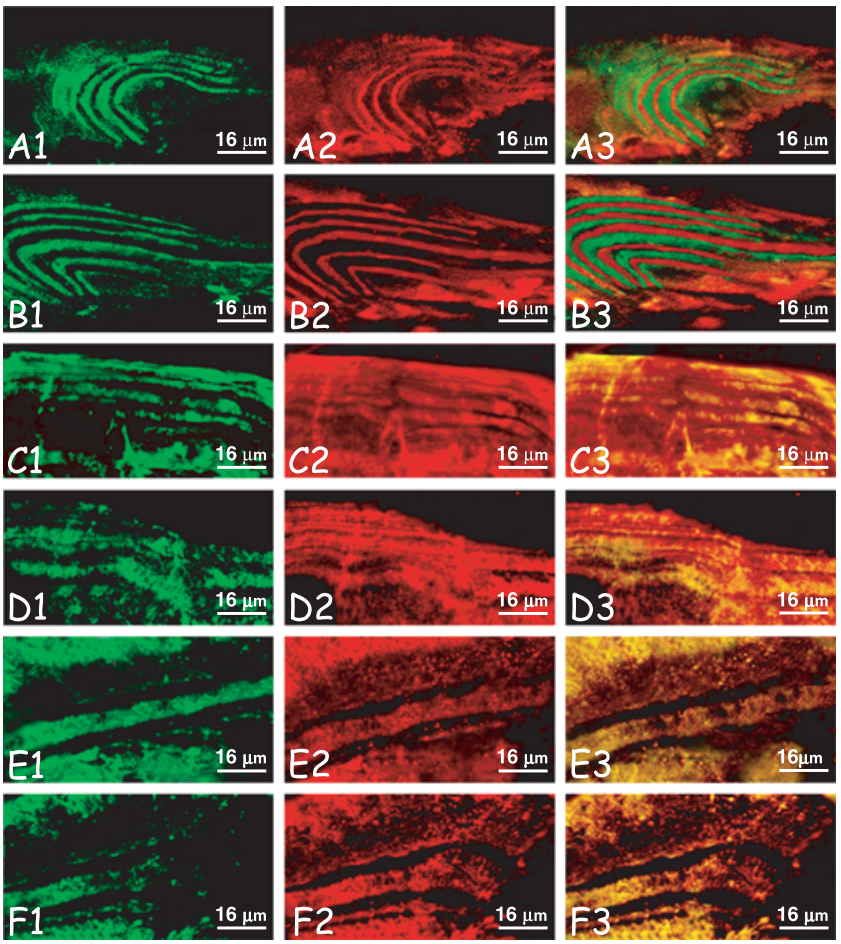

Fig. 6 Localization of CaM (red) and CaB (green) immunoreactivity in otoliths by using confocal laser scanning microscopy. (A and B) Sagitta of *C. hamatus* and *T. bernacchii*, respectively. The incremental zones are stained green by the anti-CaB antibody (A1, A3, B1 and B3), whereas the discontinuous zones are stained red by the anti-CaM antibody (A2, A3, B2 and B3). (C and D) Lapillus of *C. hamatus* and *T. bernacchii*, respectively. Both CaB (C1, C3, D1 and D3) and CaM (C2, C3, D2 and D3) are present in the incremental zones, whereas the discontinuous zones lack immunoreactivity. (E and F) Asteriscus of *C. hamatus* and *T. bernacchii*, respectively. Both CaB (E1, E3, F1 and F3) and CaM (E2, E3, F2 and F3) are present in the incremental zones, whereas the discontinuous zones lack immunoreactivity.

protrusions are usually evident (Lombarte & Castellon, 1991; Gauldie, 1993). In both *C. hamatus* and *T. bernacchii* the sensory face has a smooth and anonymous ventral region, whereas the dorsal region is characterized by ridges. These are more superficial in *C. hamatus* than in *T. bernacchii* (Avallone et al. 2003) and their surface is much smoother. Differences are also evident at the level of the collicula. These are flat in *C. hamatus* and decorated by units not observed in *T. bernacchii* where they have steep edges and a bottom showing thin depressions (Avallone et al. 2003). The collum in *C. hamatus* shows deep and round depressions but in *T. bernacchii* these are less evident and less numerous.

Differences in morphology were also seen in the utricular and lagena otoliths. In both species, the lapillus was decorated by a band of large units that are typically botryoidal in *T. bernacchii* but polygonal and irregular in *C. hamatus*. In the asteriscus the presence of a small spine is reported only in *C. hamatus*.

It is clear from the morphological results that the two species examined are closely related. However, differences are evident when the sagitta composition is considered. In *T. bernacchii*, this otolith is made exclusively of aragonite, whereas in *C. hamatus* it contains a significant vateritic component. This morph is unstable (Brunson & Chaback, 1979) and rare in nature. A vateritic asteriscus is frequent in several teleosts (Lowenstam & Weiner, 1989; Campana, 1999; Falini et al. 2005; Lenaz et al. 2006), whereas a vateritic sagitta is characteristic of ancient species such as Ciclostomata, Polypterus and sturgeons (Carlstrom, 1963). It is, however, occasionally present as an abnormality (Gauldie, 1986; Ma et al. 2007) or in juvenile (Tomàs et al. 2004; Sweeting et al. 2004) samples. Its constitutive presence in adults of a modern Notothenioid cannot be related to external factors such as stress or infections (Iguchi et al., 2003). Rather, local changes in Sr, Na and K concentrations (Gauldie, 1986, 1996; Tomàs & Geffen 2003; Ma et al. 2007) or the occurrence of a genetic mutation provide a better explanation. In the Chinook salmon, for example, it has been demonstrated that vaterite replacement is under single-locus genetic control and that this may be overridden by temperatures above or below an optimum range (Gauldie, 1986; Gauldie & Nelson, 1988). On this basis, we could suggest that, in *C. hamatus*, vaterite replaced aragonite in the sagitta while fish were adapting to progressively colder temperatures. However, it remains to be

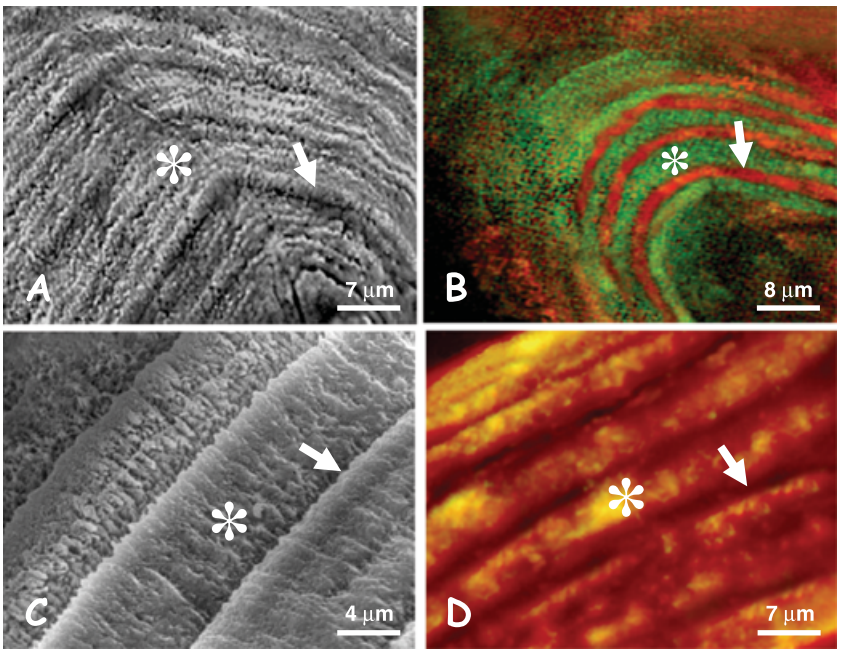

Fig. 7 Colocalization of CaM and CaB immunoreactivity with incremental (*) and discontinuous (arrow) zones in *C. hamatus* otoliths. (A and C) Scanning electron microscopy images of a mildly etched sagitta and lapillus, respectively. (B and D) Confocal laser scanning microscopy images of sagitta and lapillus as shown in Fig. 6A3 and C3.

clarified why this replacement affects the whole asteriscus, only part of the sagitta but not the lapillus.

The close similarity between *T. bernacchii* and *C. hamatus* otoliths is confirmed by our biochemical analyses. Matrices of the sagitta, lapillus and asteriscus in *C. hamatus* have the same protein patterns that are observed in the corresponding otoliths of *T. bernacchii*. An interesting aspect emerging from these observations is that, in both species, the protein pattern of the sagitta is completely different from that of the asteriscus and lapillus. Three major bands are present in the sagitta at 50, 28 and 14 kDa, whereas in the asteriscus and lapillus four major bands are visible (100, 40, 28 and 14 kDa). The utriculus and sacculus originate from different regions of the primitive otic vesicle and it is therefore not surprising that they produce otoliths with different biochemical matrices. What is surprising is that the lagena, an expansion of the sacculus, produces otoliths with a protein matrix identical to that present in utricular otoliths.

As the nature of the protein matrix and crystalline morph deposited do not correspond, our data raise another question. Although the asteriscus and lapillus have apparently identical patterns, they are made by vaterite and aragonite, respectively (or aragonite/calcite in *C. hamatus*). This evidence conflicts with the assumption that the proteins present in the matrix control calcium carbonate deposition (Lowenstam & Weiner, 1989; Pote & Ross, 1991). Further investigations will be necessary to clarify this aspect, especially considering reports that sugars (acid mucopolysaccharides, neutral mucosubstances positive to the periodic acid Schiff reaction), lipids and proteoglycans are also components of the fish otolith (Borelli et al. 2001; Tohse et al. 2008) and that these may also play a role in controlling the crystalline morph.

Our immunoblots indicate that all otoliths contain significant amounts of CaB and CaM (the 28 and 14 kDa bands, respectively), and that a significant amount of S-100 is also present in the asteriscus and lapillus (the 100 kDa band). These proteins are known to modulate the calcium balance in intra- and extracellular fluids, including the endolymph (Yamashita et al. 1995). In aragonitic otoliths, CaB in particular could control ion solubilization/deposition as reported in lizards (Piscopo et al. 2004), chicken (De Vincentiis & Marmo, 1966) and adult (Ross et al. 1980) and fetal (Veenhoff, 1969) mammals. The high concentration of calcium-binding proteins in matrices suggests that, in these Antarctic fish, all three otoliths are involved in calcium metabolism. This specialization might have occurred as an adaptation to the exceptionally stressing environmental conditions.

Laser confocal microscopy revealed that CaB is always located in incremental zones, whereas CaM is located in discontinuous zones in the sagitta and incremental zones in the lapillus and asteriscus. The significance of this difference is unclear at present.

The nature of the other bands present in gels remains completely unknown. The 54 kDa protein present in the asteriscus and lapillus may correspond to the 54 kDa protein found in the vateritic otoconia of the gar pike (Pote & Ross, 1986, 1991). The band observed around 55 kDa may correspond to otolith matrix protein-1 (OMP-1), one of the major components of fish sagittae according to Murayama et al. (2000). By contrast, the 150 kDa protein identified by Degens et al. (1969) was not detected in our otolith samples, thus clearly indicating that further investigation will be necessary.

In conclusion, the data reported here indicate that the protein composition of the otolith matrix remains unclear,

mostly due to the significant differences existing among species. Recent publications (Tohse et al. 2008; Zhang et al. 2008) provide new insights into the nature of the biomineralization of fish otoliths by describing novel matrix depositions, which may be relevant in clarifying this issue.

Acknowledgements

This work was financed by the Progetto Nazionale Ricerche in Antartide. All materials were collected during the 14th Italian Expedition by C.M.M. The scanning electron microscopy studies were carried out at the Centro Servizi di Microscopia Elettronica (CISME) of the University of Naples Federico II. The authors thank Dr Edward Howell for critical reading of the manuscript.

References

Avallone B, Balassone G, Balsamo G, et al. (2003) The otoliths of the Antarctic teleost *Trematomus bernacchii*: scanning electron microscopy and X-ray diffraction studies. *J Submicrosc Cytol Pathol* **35**, 69–76.

Avallone B, Fascio U, Senatore A, Balsamo G, Bianco PG, Marmo F (2005) The membranous labyrinth during larval development in lamprey (*Lampetra planeri*, Bloch, 1784). *Hear Res* **201**, 37–43.

Balsamo G, Avallone B, Del Genio F, Marmo F (2000) Calcification processes in the chick otoconia and calcium binding proteins: patterns of tetracycline incorporation and calbindin D28 K distribution. *Hear Res* **148**, 1–8.

Bèlanger LF (1960) Development, structure and composition of the otolithic organs of the rat. In *Calcification in Biological Systems* (ed. Sognnaes RF), pp. 151–162. Washington, DC: American Association of Advanced Science.

Borelli G, Mayer-Gostan N, De Pontual H, Boeuf G, Payan P (2001) Biochemical relationships between endolymph and otolith matrix in the trout (Oncorhynchus mykiss) and turbot (Psetta maxima). *Calcif Tissue Int* **69**(6), 356–364.

Brunson RJ, Chaback JJ (1979) Vaterite formation during coal liquification. *Chem Geol* **25**, 333–338.

Campana SE (1999) Chemistry and composition of fish otoliths: pathways, mechanism and applications. *Mar Ecol Prog Ser* **188**, 263.

Carlstrom D (1963) A crystallographic study of vertebrate otoliths. *Biol Bull* **125**, 441–463.

Coppens AG, Resibois A, Poncelet L (2000) Immunolocalization of calbindin D28 K and calretinin in the dog cochlea during postnatal development. *Hear Res* **145**, 101–110.

De Vincentiis M, Marmo F (1966) The $45Ca^{2+}$ turnover in the membranous labyrinth of chick embryo during development. *J Embryol Exp Morphol* **15**, 349–354.

Degens ET, Deuser WG, Haedrich RL (1969) Molecular structure and composition of fish otoliths. *Mar Biol* **2**, 105–113.

Falini G, Fermani S, Vanzo S, Miletic M, Zaffino G (2005) Influence on the formation of aragonite or vaterite by otolith macromolecules. *Eur J Inorg Chem* **1**, 162–167.

Fay RR (1984) The goldfish ear codes the axis of acoustic particle motion in three dimension. *Science* **225**, 951–953.

Furness DN, Karkanevatos A, West B, Hackney CM (2002) An immunogold investigation of the distribution of calmodulin in the apex of cochlear hair cells. *Hear Res* **173**, 10–20.

Gauldie RW (1986) Vaterite otoliths from chinook salmon (*Oncorhynchus tshawytscha*). *New Zeal J Mar Fresh Res* **20**, 209–217.

Gauldie RW (1993) Polymorphic crystalline structure of fish otoliths. *J Morphol* **218**, 1–28.

Gauldie RW (1996) Effects of temperature and vaterite replacement on the chemistry of metal ions in the otoliths of Oncorhynchus tshawytscha. *Can J Fish Aquat Sci* **53**, 2015–2026.

Gauldie RW, Nelson DGA (1988) Aragonite twinning and neuroprotein secretion are the cause of daily growth rings in fish otoliths. *Comp Biochem Physiol* **90**, 501–590.

Gil-Loyzaga P, Raymond J, Gabrion J (1985) Carbohydrates detected by lectins in the vestibular organs. *Hear Res* **18**, 269–272.

Henle J (1873) Quoted by S. Rudinger in Manual of human and comparative histology (ed. Stricker S), vol. 3. pp. 122. London: New Sydenham Society.

Hiel H, Navaratnam DS, Oberholtzer JC, Fuchs PA (2002) Topological and developmental gradients of calbindin expression in the chick's inner ear. *J Assoc Res Otolaryngol* **3**, 1–15.

Iguchi K, Ogawa K, Nagae M, Ito F (2003) The influence of rearing density on stress response and disease susceptibility of ayu (Plecoglossus altivelis). *Aquaculture* **220**, 515–523.

Karita K, Nishizaki K, Nomiya S, Masuda Y (1999) Calbindin and calmodulin localization in the developing vestibular organ of the musk shrew (*Suncus murinus*). *Acta Otolaryngol Suppl* **540**, 16–21.

Laemmli UK (1970) Cleavage of structural proteins during the assembly of the head of bacteriophage T4. *Nat Lond* **227**, 680–685.

Lenaz D, Miletic M, Pizzul E, Vanzo S, Adami G (2006) Minerology and geochemistry of otoliths in freshwater fish from Northern Italy. *Eur J Mineral* **18**, 143–148.

Lewis ER, Nemanic P (1972) Scanning electron microscope observations of saccular ultrastructure in the Mudpuppy (*Necturus maculosus*). *Z Zellforschung* **123**, 441–457.

Lombarte A, Castellon A (1991) Interspecific and intraspecific otolith variability in the genus Merluccius as determined by image analysis. *Can J Zool* **69**, 2442–2449.

Lombarte A, Rucabado J, Matallanas J, Lloris D (1991) Taxonomia numerica de Nototheniidae en base a la forma de los otolitos. *Sci Mar* **55**, 413–418.

Lowenstam HA, Weiner S (1989) *On Biomineralization*. New York: Oxford University Press.

Ma T, Kuroki M, Miller MJ (2007) Morphology and microchemistry of abnormal otoliths in the ayu, Plecoglossus altivelis. *Environ Biol Fish*. doi 10.1007/s10641-007-9308-4.

Marmo F, De Vincentiis M, Materazzi G (1964) Caratterizzazione istochimica dei mucopolisaccaridi di alcune strutture del labirinto membranoso dell'embrione di pollo. *Riv Istoch* **10**, 733–742.

Merril CR, Goldman D, Van Keuren ML (1984) Gel protein stains: silver stains. *Meth Enzymol* **104**, 441–447.

Morales-Nin B (1985) Caracteristicas de los otolitos cristalinos de *Genypterus capensis* (Smith, 1847) (Pisces: Ophidiidae). *Inv Pesq* **49**, 379–386.

Murayama E, Okuno A, Ohira T, Takagi Y, Nagasawa H (2000) Molecular cloning and expression of an otolith matrix protein cDNA from the rainbow trout, *Oncorhynchus mykiss*. *Comp Biochem Physiol B Biochem Mol Biol* **126**, 511–520.

Nakazawa K (2001) Ultrastructural localization of calmodulin in gerbil cochlea by immunogold electron microscopy. *Hear Res* **151**, 133–140.

Parker GH (1908) Structure and functions of the ear of the squeteague. *Bull Bureau Fish* **27**, 1213–1225.

Piscopo M, Avallone B, D'Angelo L, Fascio U, Balsamo G, Marmo F (2004) Localization of calbindin D28 K in the otoconia of lizard *Podarcis sicula*. *Hear Res* **189**, 76–82.

Piscopo M, Balsamo G, Mutone R, Avallone B, Marmo F (2003) Calbindin D28 K is a component of the organic matrix in lizard *Podarcis sicula* otoconia. *Hear Res* **178**, 89–94.

Pote KG, Ross MD (1986) Ultrastructural morphology and protein content of the internal organic material of rat otoconia. *J Ultr Mol Struct Res* **95**, 61–70.

Pote KG, Ross MD (1991) Each otoconia polymorph has a protein unique to that polymorph. *Comp Biochem Physiol B* **98**, 287–295.

Ross MD, Pote KG, Cloke PL, Corson C (1980) In vitro $45Ca^{2+}$ uptake and exchange in otoconia complexes in high and low K^+/Na^+ fluids. *Physiologist* **23** (Suppl. 6), 129–130.

Ross MD, Pote KG, Perini F (1985) Analytical studies of the organic material of otoconial complexes, including its aminoacid and carbohydrate composition. In Auditory biochemistry (ed. Drescher DG), pp. 500–514. Springfield, IL, Thomas.

Schuijf A (1981) Models of acoustic localization. In *Hearing and Sound Communication in Fishes* (eds Tavolga WN, Popper AN, Fay RR), pp. 267–310. Berlin: Springer-Verlag.

Sweeting RM, Beamish RJ, Neville CM (2004) Crystalline otoliths in teleosts: comparisons between hatchery and wild coho salmon (Oncorhynchus kisutch) in the Strait of Georgia. *Rev Fish Biol Fisheries* **14**, 361–369.

Tohse H, Takagi Y, Nagasawa H (2008) Identification of a novel matrix protein contained in a protein aggregate associated with collagen in fish otoliths. *FEBS J* **275** (10), 2512–2523.

Tomàs J, Geffen AJ (2003) Morphometry and composition of aragonite and vaterite otoliths of deformed laboratory reared juvenile herring from two populations. *J Fish Biol* **63**, 1383–1401.

Tomàs J, Geffen AG, Allen IS, Berges J (2004) Analysis of the soluble matrix in vaterite otoliths of juvenile herring (Clupea harengus): do crystalline otoliths have less protein? *Comp Biochem Physiol A Mol Integr Physiol* **139**, 301–308.

Usami S, Shinkawa H, Inoue Y, Kanzaki J, Anniko M (1995) Calbindin D28 K localization in the primate inner ear. *ORL* **57**, 94–99.

Veenhoff VB (1969) The development of statoconia in mice. Akademie van Wetenschappen, Afdeling Natuurkunde 2/58, no. 4. Amsterdam: N.V. North Holland.

Wislocki GB, Ladman AG (1955) Selective and histochemical staining of the otolithic membranes cupulae and tectorial membrane of the inner ear. *J Anat* **89**, 3–12.

Yamashita H, Takahashi M, Bagger-Sjoback D (1995) Expression of S-100 protein in the human fetal inner ear. *Eur Arch Otorhinolaryngol* **252**, 312–315.

Zhang F, Cai W, Sun Z, Zhang J (2008) Regular variations in organic matrix composition of small yellow croaker (*Pseudociaena polyactis*) otoliths: an in situ Raman microspectroscopy and mapping study. *Anal Bioanal Chem* **390**, 777–782.